CrossMark

High-Order Perturbation of Surfaces Algorithms for the Simulation of Localized Surface Plasmon Resonances in Two Dimensions

David P. Nicholls[1] (ID) · **Xin Tong**[1]

Abstract The capability of simulating scattering returns of electromagnetic radiation from bounded obstacles is of overwhelming importance to scientists and engineers. Furthermore, such simulations must be of both surpassing accuracy and high fidelity for many applications of interest. High-Order Spectral methods deliver highly accurate simulations with a relatively small number of degrees of freedom, while interfacial formulations which utilize these discretizations have orders of magnitude smaller execution times and memory requirements. Among these, the High-Order Perturbation of Surfaces algorithms have proved to be a method of choice in layered media applications, and we display here how two of these-the Methods of Field Expansions and Transformed Field Expansions-extend to obstacles of bounded cross-section. In this contribution we provide not only a detailed prescription of the algorithms, but also validate the schemes and point out their benefits and shortcomings. With numerical experiments we show the remarkable efficiency, fidelity, and high-order accuracy one can achieve with implementations of these algorithms.

Keywords High-Order Spectral Methods · Linear wave scattering · Bounded obstacles · High-Order Perturbation of Surfaces Methods

1 Introduction

The capability of simulating scattering returns of electromagnetic radiation from bounded obstacles is of overwhelming importance to scientists and engineers. In the field of plasmonics alone [13,26,36,51] such crucial applications as surface enhanced Raman scattering (SERS) biosensing [60], imaging [25], and cancer therapy [14] are important examples. We refer the interested reader to any of the many surveys on the topic including Chapters 5, 9, and 10 of [26], the survey article [28], and the surveys on gold nanoparticles [33] and [24]. Due to the

---

✉ David P. Nicholls
davidn@uic.edu

1   Department of Mathematics, Statistics, and Computer Science, University of Illinois at Chicago, Chicago, IL 60607, USA

very strong plasmonic effect (the field enhancement can be several orders of magnitude) and its quite sensitive nature (the enhancement is only seen over a range of tens of nanometers in incident radiation for gold and silver particles), such simulations must be very robust and of high accuracy for many applications of interest.

In this contribution we focus upon the Localized Surface Plasmon Resonances (LSPRs) which can be induced in gold and silver nanorods with visible light, and how they change as the shapes of these rods are varied analytically away from perfectly cylindrical. In more detail, if a nanorod with cross-section shaped by $\{r = \bar{g}\}$ is composed of a noble metal (e.g., gold or silver) with a wavelength-dependent permittivity, $\epsilon_m = \epsilon_m(\lambda)$, housed in a dielectric with constant permittivity, ϵ_d, then if $\bar{g}$ is sufficiently small an LSPR is excited with incident radiation of wavelength, λ_F, that (nearly) satisfies the two-dimensional "Fröhlich condition" [26]

$$\mathrm{Re}\,[\epsilon_m(\lambda)] = -\epsilon_d. \tag{1.1}$$

However, if the cross-section of the rod is specified by

$$r = \bar{g} + \varepsilon f(\theta),$$

for some smooth function f and ε sufficiently small, then the value $\lambda_F = \lambda_F(\varepsilon)$ will change and, as we shall see, our novel approach is ideally suited to study its evolution.

All of the classical numerical algorithms have been utilized for the simulation of this problem (e.g., Finite Difference Methods [23,59], Finite Element Methods [20,21], Discontinuous Galerkin Methods [19], Spectral Element Methods [12], and Spectral Methods [3,10,16]), but we have recently argued [38,41] that such *volumetric* approaches are greatly disadvantaged with an unnecessarily large number of unknowns for the piecewise homogeneous problems we consider here. Interfacial methods based upon Integral Equations (IEs) [11] are a natural candidate but, as we have pointed out these also face difficulties. Most of these have been addressed in recent years through (i) the use of sophisticated quadrature rules to deliver High-Order Spectral accuracy, (ii) the design of preconditioned iterative solvers with suitable acceleration [17]. Consequently, they are a compelling alternative (see, e.g., the survey article of [58] for more details), however, two properties render them non-competitive for the *parameterized* problems we consider as compared with the methods we advocate here:

1. For geometries specified by the real value ε (here the deviation of an obstacle of bounded cross-section from cylindrical), an IE solver will return the scattering returns only for a particular value of ε. If this value is changed then the solver must be run again.
2. The dense, non-symmetric positive definite systems of linear equations which must be inverted with each simulation.

As we advocated in [38,41] a "High Order Perturbation of Surfaces" (HOPS) approach can effectively address these concerns. More specifically, we argued for the method of Field Expansions (FE) which trace their roots to the low-order calculations of Rayleigh [52] and Rice [53]. The high-order version was first investigated by Bruno and Reitich [4–7] and later enhanced and stabilized by the first author and Reitich [45,46], the first author and Nigam [40], and the first author and Shen [47], resulting in the Method of Transformed Field Expansions (TFE). These formulations maintain the advantageous properties of classical IE formulations (e.g., surface formulation and exact enforcement of far-field conditions) while avoiding the shortcomings listed above:

1. As HOPS methods are built upon expansions in the deformation parameter, ε, once the Taylor coefficients are known for the scattering quantities, it is simply a matter of

summing these (rather than beginning a new simulation) for any given choice of ε to recover the returns.

2. Due to the perturbative nature of the scheme, at every Taylor order, one need only invert a single, sparse operator corresponding to the cylindrical-interface, order-zero approximation of the problem.

Our new approach is quite closely related to the work of Bruno and Reitich [7] who studied the same problem in the three-dimensional context of nanospheres. The current contribution differs in a number of ways beginning with its two-dimensional character which requires the study of different Hankel functions. In addition we utilize a formulation in terms of Dirichlet–Neumann Operators (DNOs) first described in [37] which permits the immediate simulation by either of the classical HOPS methods, FE [4–7] or Operator Expansions [9,29–32,34,35], or the stabilized TFE approach [40,46,47]. In this contribution we provide not only a detailed prescription of the algorithm (utilizing both the FE and TFE recursions), but also validate the scheme and point out its benefits and shortcomings. With numerical experiments we show the remarkable efficiency, fidelity, and high-order accuracy one can achieve with an implementation of this algorithm.

The rest of the paper is organized as follows: In Sect. 2 we recall the governing equations for linear waves reflected and transmitted by a cylindrical obstacle, with particular attention paid to transparent boundary conditions in Sect. 2.1. We give a novel boundary formulation of the resulting problem in Sect. 3 and using this we study the classical problem of scattering by a rod in Sect. 3.1, and its generalization to non-trivial geometries in Sect. 3.2. The FE method is explained in Sect. 3.3, while its TFE analogue is derived in Sect. 3.4. In Sect. 4 we discuss our numerical results, including the Method of Manufactured Solutions to validate our code in Sect. 4.1, implementation and error measurement in Sect. 4.2, and a convergence study in Sect. 4.3. We end with simulations of nanorods in Sect. 4.4, and concluding remarks in Sect. 5.

2 Governing Equations

We consider a y-invariant obstacle of bounded cross-section as displayed in Fig. 1. In this paper we assume a dielectric material of refractive index n^u (e.g., air) occupies the unbounded exterior, and a metal of refractive index n^w (e.g., gold or silver) fills the bounded interior; however, our formulation can accommodate arbitrary materials in either domain. The interface between the two domains is described in polar coordinates, $\{x = r\cos(\theta), z = r\sin(\theta)\}$, by the graph $r = \bar{g} + g(\theta)$ so that the exterior domain is specified by

$$S^u := \{r > \bar{g} + g(\theta)\},$$

while the interior domain is given by

$$S^w := \{r < \bar{g} + g(\theta)\}.$$

The superscripts are chosen to conform to the notation of previous work by the author [37,41,48]. Obviously, the cylindrical geometry demands that the interface be 2π-periodic, $g(\theta + 2\pi) = g(\theta)$. The structure is illuminated by monochromatic plane-wave incident radiation of frequency ω and wavenumber $k^u = n^u\omega/c_0 = \omega/c^u$ (c_0 is the speed of light), aligned with the corrugations of the obstacle. We consider the reduced incident fields of incidence angle ϕ

Fig. 1 Plot of the cross-section of a metallic nanorod (occupying S^w) shaped by $r = \bar{g} + \varepsilon \cos(4\theta)$ ($\varepsilon = \bar{g}/5$) housed in a dielectric (occupying S^u) under plane-wave illumination with wavenumber $(\alpha, -\gamma^u)$
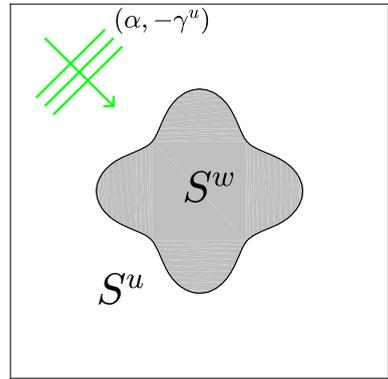
$$\mathbf{E}^{\text{inc}} = \mathbf{A}e^{i\alpha x - i\gamma^u z} = \mathbf{A}e^{ir(\alpha \cos(\theta) - i\gamma^u \sin(\theta))},$$
$$\mathbf{H}^{\text{inc}}(x, z) = \mathbf{B}e^{i\alpha x - i\gamma^u z} = \mathbf{B}e^{ir(\alpha \cos(\theta) - i\gamma^u \sin(\theta))},$$
$$\alpha = k^u \sin(\phi), \quad \gamma^u = k^u \cos(\phi),$$

where time dependence of the form $\exp(-i\omega t)$ has been factored out. The geometry demands that the reduced electric and magnetic fields, $\{\mathbf{E}, \mathbf{H}\}$, be 2π-periodic in θ. To close the problem, we specify that the scattered radiation is "outgoing" in S^u and bounded in S^w.

It is well-known (see, e.g., [50]) that in this two-dimensional setting, the time-harmonic Maxwell equations decouple into two scalar Helmholtz problems which govern the transverse electric (TE) and transverse magnetic (TM) polarizations. We define the invariant (y) directions of the scattered (electric or magnetic) fields by $\{u(r, \theta), w(r, \theta)\}$ in S^u and S^w, respectively, and the incident radiation in the outer domain by $u^{\text{inc}}(r, \theta)$.

In light of all of this, we are led to seek outgoing/bounded, 2π-periodic solutions of

$$\Delta u + (k^u)^2 u = 0, \qquad\qquad r > \bar{g} + g(\theta), \qquad\qquad (2.1a)$$
$$\Delta w + (k^w)^2 w = 0, \qquad\qquad r < \bar{g} + g(\theta), \qquad\qquad (2.1b)$$
$$u - w = \zeta, \qquad\qquad r = \bar{g} + g(\theta), \qquad\qquad (2.1c)$$
$$\partial_N u - \tau^2 \partial_N w = \psi, \qquad\qquad r = \bar{g} + g(\theta), \qquad\qquad (2.1d)$$

where the Dirichlet and Neumann data are

$$\zeta(\theta) := \left[-u^{\text{inc}}\right]_{r=\bar{g}+g(\theta)} = -e^{i(\bar{g}+g(\theta))(\alpha \cos(\theta) - \gamma^u \sin(\theta))} \qquad (2.1e)$$

$$\psi(\theta) := \left[-\partial_N u^{\text{inc}}\right]_{r=\bar{g}+g(\theta)}$$
$$= \Bigg[(\bar{g} + g)(i\alpha \cos(\theta) - i\gamma^u \sin(\theta))$$
$$- \frac{g'}{\bar{g} + g}(-i\alpha(\bar{g} + g)\sin(\theta) - i\gamma^u(\bar{g} + g)\cos(\theta))\Bigg]\zeta. \qquad (2.1f)$$

In these

$$\partial_N = \hat{r}(\bar{g} + g)\partial_r - \hat{\theta}\left(\frac{g'}{\bar{g} + g}\right)\partial_\theta,$$

for unit vectors in the radial ($\hat{r}$) and angular ($\hat{\theta}$) directions, and

$$\tau^2 = \begin{cases} 1, & \text{TE}, \\ (k^u/k^w)^2 = (n^u/n^w)^2, & \text{TM}, \end{cases}$$

where $\gamma^w = k^w \cos(\phi)$. The case of TM polarization is of extraordinary importance in the study of SPRs [51] and thus we concentrate our attention on the TM case from here.

2.1 Transparent Boundary Conditions

Regarding the Outgoing Wave Condition (OWC), commonly known as the Sommerfeld Radiation Condition [11], and Boundedness Boundary Condition (BBC), we introduce the circles $\{r = R^o\}$ and $\{r = R_i\}$, where

$$R^o > \bar{g} + |g|_{L^\infty}, \quad 0 < R_i < \bar{g} - |g|_{L^\infty},$$

define the domains

$$S^o := \{r > R^o\}, \quad S_i := \{r < R_i\},$$

and note that we can find periodic solutions of the relevant Helmholtz problems on these domains given generic Dirichlet data, say $\xi(\theta)$ and $\mu(\theta)$. For this we use the exact solutions [11]

$$u(r, \theta) = \sum_{p=-\infty}^{\infty} \hat{\xi}_p \frac{H_p(k^u r)}{H_p(k^u R^o)} e^{ip\theta}, \quad w(r, \theta) = \sum_{p=-\infty}^{\infty} \hat{\mu}_p \frac{J_p(k^w r)}{J_p(k^w R_i)} e^{ip\theta}, \qquad (2.2)$$

where, J_p is the pth Bessel function and H_p is the pth Hankel function of the first kind. We note that

$$u(R^o, \theta) = \sum_{p=-\infty}^{\infty} \hat{\xi}_p e^{ip\theta}, \quad w(R_i, \theta) = \sum_{p=-\infty}^{\infty} \hat{\mu}_p e^{ip\theta}.$$

With these formulas we can compute the *outward-pointing* Neumann data at the artificial boundaries

$$-\partial_r u(R^o, \theta) = \sum_{p=-\infty}^{\infty} -k^u \hat{\xi}_p \frac{H_p'(k^u R^o)}{H_p(k^u R^o)} e^{ip\theta} =: T^{(u)}[\xi(\theta)],$$

$$\partial_r w(R_i, \theta) = \sum_{p=-\infty}^{\infty} k^w \hat{\mu}_p \frac{J_p'(k^w R_i)}{J_p(k^w R_i)} e^{ip\theta} =: T^{(w)}[\mu(\theta)].$$

These define the order-one Fourier multipliers $\{T^{(u)}, T^{(w)}\}$.

With the operator $T^{(u)}$ it is not difficult to see that periodic, outward propagating solutions to the Helmholtz equation

$$\Delta u + (k^u)^2 u = 0, \quad r > \bar{g} + g(\theta),$$

equivalently solve

$$\Delta u + (k^u)^2 u = 0, \qquad\qquad \bar{g} + g(\theta) < r < R^o, \qquad (2.3a)$$
$$\partial_r u + T_u[u] = 0, \qquad\qquad r = R^o. \qquad\qquad\qquad (2.3b)$$

Similarly, one can show that periodic, bounded solutions to the Helmholtz equation

$$\Delta w + (k^w)^2 w = 0, \quad r < \bar{g} + g(\theta),$$

equivalently solve

$$\Delta w + \left(k^w\right)^2 w = 0, \qquad\qquad R_i < r < \bar{g} + g(\theta), \qquad (2.4a)$$

$$\partial_r w - T^{(w)}[w] = 0, \qquad\qquad r = R_i. \qquad\qquad (2.4b)$$

3 Boundary Formulation

We follow [37,39] and reduce our degrees of freedom to the following surface unknowns, the (outer and inner) Dirichlet traces

$$U(\theta) := u(\bar{g} + g(\theta), \theta), \quad W(\theta) := w(\bar{g} + g(\theta), \theta),$$

and their (exterior, outer and inner) Neumann counterparts

$$\tilde{U}(\theta) := -(\partial_N u)(\bar{g} + g(\theta), \theta), \quad \tilde{W}(\theta) := (\partial_N w)(\bar{g} + g(\theta), \theta).$$

From these one could recover the scattered field at any point with a suitable integral formula [15]. Thus, the governing equations reduce to the boundary conditions

$$U - W = \zeta, \quad -\tilde{U} - \tau^2 \tilde{W} = \psi. \qquad (3.1)$$

At this point we have two equations for four unknowns, however, the pairs $\{U, \tilde{U}\}$ and $\{W, \tilde{W}\}$ are clearly related, and we make this clear through the introduction of Dirichlet–Neumann operators (DNOs). For this we make the following definitions.

Definition 3.1 Given a sufficiently smooth deformation $g(\theta)$, the unique periodic solution of

$$\Delta u + \left(k^u\right)^2 u = 0, \qquad\qquad \bar{g} + g(\theta) < r < R^o, \qquad (3.2a)$$

$$u = U, \qquad\qquad r = \bar{g} + g(\theta), \qquad\qquad (3.2b)$$

$$\partial_r u + T^{(u)}[u] = 0, \qquad\qquad r = R^o, \qquad\qquad (3.2c)$$

defines the Dirichlet–Neumann Operator

$$G^{(u)}[U] = G^{(u)}(R^o, \bar{g}, g)[U] := \tilde{U}. \qquad (3.3)$$

An analogous definition will presently be made on the interior domain, $\{R_i < r < \bar{g} + g(\theta)\}$, however, care is required. It is well known [11] that the governing Helmholtz equation, (2.1b), is not uniquely solvable at a "Dirichlet eigenvalue" and so we must avoid these. For example, in the case $g \equiv 0$ the exact solution is given by (2.2) with R_i replaced by $\bar{g}$. It is easy to see that one will not be able to uniquely solve the Dirichlet problem when $J_p(k^w \bar{g}) = 0$ for *any* $p \in \mathbf{Z}$. Such configurations, and their generalizations to $g \not\equiv 0$, are the Dirichlet eigenvalues we must avoid. By contrast, the exterior problem has no such obstruction and can always be shown to be uniquely solvable [11].

Definition 3.2 Given a sufficiently smooth deformation $g(\theta)$, if we are not at a Dirichlet eigenvalue of the Laplacian on $\{r < \bar{g} + g(\theta)\}$, the unique periodic solution of

$$\Delta w + \left(k^w\right)^2 w = 0, \qquad\qquad R_i < r < \bar{g} + g(\theta), \qquad (3.4a)$$

$$w = W, \qquad\qquad r = \bar{g} + g(\theta), \qquad\qquad (3.4b)$$

$$\partial_r w - T^{(w)}[w] = 0, \qquad\qquad r = R_i, \qquad\qquad (3.4c)$$

defines the Dirichlet–Neumann Operator

$$G^{(w)}[W] = G^{(w)}(R_i, \bar{g}, g)[W] := \tilde{W}. \qquad (3.5)$$

In terms of these operators the boundary conditions, (3.1), become

$$U - W = \zeta, \quad -G^{(u)}[U] - \tau^2 G^{(w)}[W] = \psi.$$

The first of these can be used to eliminate W,

$$W = U - \zeta,$$

so that the latter equation becomes

$$-G^{(u)}[U] - \tau^2 G^{(w)}[U - \zeta] = \psi,$$

or

$$(G^{(u)} + \tau^2 G^{(w)})U = -\psi + \tau^2 G^{(w)}[\zeta]. \qquad (3.6)$$

3.1 The Trivial Configuration: LSPR Condition

Before specifying our full algorithm, we show how our formulation delivers the classical solution for plane wave scattering by a cylindrical obstacle. For this we investigate (3.6) in the case $g \equiv 0$,

$$\left(G_0^{(u)} + \tau^2 G_0^{(w)} \right) [U] = -\psi_0 + \tau^2 G_0^{(w)}[\zeta_0]. \qquad (3.7)$$

It is not difficult to see that, in this trivial configuration, the solutions to (3.2) and (3.4) are, (c.f. (2.2)),

$$u(r, \theta) = \sum_{p=-\infty}^{\infty} \hat{U}_p \frac{H_p(k^u r)}{H_p(k^u \bar{g})} e^{ip\theta}, \quad w(r, \theta) = \sum_{p=-\infty}^{\infty} \hat{W}_p \frac{J_p(k^w r)}{J_p(k^w \bar{g})} e^{ip\theta}, \qquad (3.8)$$

respectively. From these we find for (3.3)

$$G_0^{(u)}[U] = \sum_{p=-\infty}^{\infty} \hat{U}_p (-k^u \bar{g}) \frac{H_p'(k^u \bar{g})}{H_p(k^u \bar{g})} e^{ip\theta} =: -(k^u \bar{g}) \frac{H_D'(k^u \bar{g})}{H_D(k^u \bar{g})} U,$$

and for (3.5)

$$G_0^{(w)}[W] = \sum_{p=-\infty}^{\infty} \hat{W}_p (k^w \bar{g}) \frac{J_p'(k^w \bar{g})}{J_p(k^w \bar{g})} e^{ip\theta} =: (k^w \bar{g}) \frac{J_D'(k^w \bar{g})}{J_D(k^w \bar{g})} W,$$

which define the order-one Fourier multipliers

$$G_0^{(u)} = -(k^u \bar{g}) \frac{H_D'(k^u \bar{g})}{H_D(k^u \bar{g})}, \quad G_0^{(w)} = (k^w \bar{g}) \frac{J_D'(k^w \bar{g})}{J_D(k^w \bar{g})},$$

respectively.

Returning to (3.7), using the solution (3.8), we find the solution at each wavenumber

$$\hat{U}_p = \frac{-(\hat{\psi}_0)_p + \tau^2 (k^w \bar{g}) \frac{J_p'(k^w \bar{g})}{J_p(k^w \bar{g})} (\hat{\zeta}_0)_p}{-(k^u \bar{g}) \frac{H_p'(k^u \bar{g})}{H_p(k^u \bar{g})} + \tau^2 (k^w \bar{g}) \frac{J_p'(k^w \bar{g})}{J_p(k^w \bar{g})}}$$

$$= \frac{H_p(k^u \bar{g}) J_p(k^w \bar{g}) (\hat{\psi}_0)_p - \tau^2 (k^w \bar{g}) H_p(k^u \bar{g}) J_p'(k^w \bar{g}) (\hat{\zeta}_0)_p}{(k^u \bar{g}) J_p(k^w \bar{g}) H_p'(k^u \bar{g}) - \tau^2 (k^w \bar{g}) H_p(k^u \bar{g}) J_p'(k^w \bar{g})}.$$

It is clear that solvability of this system hinges on

$$\Delta_p := -\tau^2 (k^w \bar{g}) H_p(k^u \bar{g}) J_p'(k^w \bar{g}) + (k^u \bar{g}) H_p'(k^u \bar{g}) J_p(k^w \bar{g}).$$

We study this in the "small radius" (quasistatic) limit [26], $k^u \bar{g} \ll 1$ and $k^w \bar{g} \ll 1$. For this we recall that, for p a positive integer,

$$J_p(z) \sim \frac{z^p}{2^p p!}, \qquad\qquad\qquad z \to 0,$$

$$H_p(z) \sim i Y_p(z) \sim \frac{i(p-1)!}{\pi} \frac{2^p}{z^p}, \qquad\qquad z \to 0,$$

$$J_p'(z) \sim \frac{z^{p-1}}{2^p (p-1)!}, \qquad\qquad\qquad z \to 0,$$

$$H_p'(z) \sim i Y_p'(z) \sim -\frac{ip!}{\pi} \frac{2^p}{z^{p+1}}, \qquad\qquad z \to 0,$$

so that

$$\Delta_p \sim -\tau^2 k^w \bar{g} \left(\frac{i(p-1)!}{\pi} \frac{2^p}{(k^u \bar{g})^p} \right) \left(\frac{(k^w \bar{g})^{p-1}}{2^p (p-1)!} \right) + k^u \bar{g} \left(-\frac{ip!}{\pi} \frac{2^p}{(k^u \bar{g})^{p+1}} \right) \left(\frac{(k^w \bar{g})^p}{2^p p!} \right)$$

$$= -\frac{i}{\pi} (\tau^2 + 1) \left(\frac{k^w}{k^u} \right)^p.$$

This demonstrates that, in the small radius limit, $\Delta_p \approx 0$ if $\tau^2 = -1$, or

$$\epsilon^{(u)} = -\text{Re}\{\epsilon^{(w)}\} - i\text{Im}\{\epsilon^{(w)}\},$$

where we have used $\tau^2 = \epsilon^{(u)}/\epsilon^{(w)}$. Since $\epsilon^{(u)}$ is real this can never be exactly satisfied, however, if the Fröhlich condition

$$\epsilon^{(u)} = -\text{Re}\{\epsilon^{(w)}\}, \tag{3.9}$$

c.f. (1.1), is verified then it can "almost" be true. We note that this is *different* from the three dimensional Fröhlich condition for nanoparticles

$$\epsilon^{(u)} = -2\text{Re}\{\epsilon^{(w)}\}.$$

3.2 Non-trivial Configurations

Of course the exact solution to the trivial configuration described above is classical [27] and the scientific applications of this have been explored in great depth. Of greater current interest is the non-trivial case where $g \not\equiv 0$, and we can use a High-Order Perturbation of Surfaces (HOPS) scheme to simulate scattering returns if we view $g(\theta) = \varepsilon f(\theta)$.

For ε sufficiently small and f sufficiently smooth the operators, $\{G^{(u)}, G^{(w)}\}$, and data, $\{\zeta, \psi\}$, can be shown to be analytic in ε so that the following Taylor series are strongly convergent

$$\{G^{(u)}, G^{(w)}, \zeta, \psi\} = \{G^{(u)}, G^{(w)}, \zeta, \psi\}(\varepsilon f) = \sum_{n=0}^{\infty} \left\{ G_n^{(u)}, G_n^{(w)}, \zeta_n, \psi_n \right\} \varepsilon^n.$$

Remark 3.3 In fact, appealing to the work of the first author and Reitich [42,44], Nigam [40], and Hu [18], we can safely claim that surface perturbations of C^2 (and even Lipschitz) smoothness can be accommodated, and the domain of applicability be extended to all *real* values of ε (up to topological obstruction).

Consequently, the resulting scattered field can be shown to be analytic as well

$$U = U(\varepsilon f) = \sum_{n=0}^{\infty} U_n \varepsilon^n.$$

Furthermore, it is straightforward to identify a recursive formula for U_n. For this we write (3.6) as

$$\left(\sum_{n=0}^{\infty} \left(G_n^{(u)} + \tau^2 G_n^{(w)} \right) \varepsilon^n \right) \left[\sum_{m=0}^{\infty} U_m \varepsilon^m \right] = - \sum_{n=0}^{\infty} \psi_n \varepsilon^n + \tau^2 \left(\sum_{n=0}^{\infty} G_n^{(w)} \varepsilon^n \right) \left[\sum_{m=0}^{\infty} \zeta_m \varepsilon^m \right],$$

and equating at order $\mathcal{O}(\varepsilon^n)$,

$$\left(G_0^{(u)} + \tau^2 G_0^{(w)} \right) U_n = - \psi_n + \tau^2 \sum_{m=0}^{n} G_{n-m}^{(w)} [\zeta_m] - \sum_{m=0}^{n-1} \left(G_{n-m}^{(u)} + \tau^2 G_{n-m}^{(w)} \right) [U_m]. \quad (3.10)$$

At order zero we recover the trivial shape calculation, (3.7), from the previous section, while higher order corrections can be recovered from (3.10). We note that at every perturbation order we must invert the *same* linear operator, $(G_0^{(u)} + \tau^2 G_0^{(w)})$, which renders the algorithm extremely computationally efficient.

All that remains is to specify forms for the data, $\{\zeta_n, \psi_n\}$, and operators, $\{G_n^{(u)}, G_n^{(w)}\}$. For the former it is easy to show that

$$\zeta_n(\theta) = - e^{\bar{g}(i\alpha \cos\theta - i\gamma^u \sin\theta)} (i\alpha \cos\theta - i\gamma^u \sin\theta)^n F_n,$$
$$\psi_n(\theta) = \bar{g}(i\alpha \cos\theta - i\gamma^u \sin\theta)\zeta_n(\theta)$$
$$\quad + \left[f(i\alpha \cos\theta - i\gamma^u \sin\theta) - (f')(-i\alpha \sin\theta - i\gamma^u \cos\theta) \right] \zeta_{n-1}(\theta),$$

where

$$F_n = F_n(\theta) := \frac{(f(\theta))^n}{n!}.$$

For the latter we appeal to the FE and TFE methods [4–6,45,46] which we briefly explain here for completeness (see also [40]).

3.3 The Method of Field Expansions

The method of Field Expansions begins with the supposition that the scattered fields, $\{u, w\}$, depend analytically upon ε. Focusing upon the field u in the outer domain, $\{r > \bar{g} + \varepsilon f(\theta)\}$, this implies that

$$u = u(r, \theta; \varepsilon) = \sum_{n=0}^{\infty} u_n(r, \theta) \varepsilon^n.$$

Upon insertion of this into (3.2) one finds that the u_n must be 2π-periodic, outward-propagating solutions of the elliptic boundary value problem

$$\Delta u_n + \left(k^u \right)^2 u_n = 0, \qquad\qquad\qquad \bar{g} < r < R^o, \qquad (3.11a)$$

$$u_n(\bar{g}, \theta) = \delta_{n,0} U - \sum_{\ell=0}^{n-1} \frac{f^{n-\ell}}{(n-\ell)!} \partial_r^{n-\ell} u_\ell(\bar{g}, \theta), \qquad r = \bar{g}, \qquad (3.11b)$$

$$\partial_r u_n + T^{(u)}[u_n] = 0, \qquad\qquad\qquad r = R^o, \qquad (3.11c)$$

where $\delta_{n,\ell}$ is the Kronecker delta function. The exact solutions (3.8) are

$$u_n(r, \theta) = \sum_{p=-\infty}^{\infty} \hat{u}_{n,p} \frac{H_p(k^u r)}{H_p(k^u \bar{g})} e^{ip\theta},$$

and the $\hat{u}_{n,p}$ are determined recursively from the boundary conditions, (3.11b), beginning, at order zero, with

$$\hat{u}_{0,p} = \hat{U}_p.$$

From this the DNO, (3.3), can be computed from

$$G^{(u)}[U] = -(\partial_N u)(\bar{g} + g(\theta), \theta)$$

$$= \sum_{n=0}^{\infty} \sum_{p=-\infty}^{\infty} \left\{ -k^u(\bar{g} + \varepsilon f) \frac{H'_p(k^u(\bar{g} + \varepsilon f))}{H_p(k^u \bar{g})} \right.$$

$$\left. + \frac{\varepsilon f'}{(\bar{g} + \varepsilon f)} (ip) \frac{H_p(k^u(\bar{g} + \varepsilon f))}{H_p(k^u \bar{g})} \right\} \hat{u}_{n,p} e^{ip\theta} \varepsilon^n,$$

expanding the Hankel functions $H'_p(k^u(\bar{g} + \varepsilon f))$ and $H_p(k^u(\bar{g} + \varepsilon f))$ in power series in ε, and equating like powers of ε. This results in

$$G_n^{(u)}(f)[U] = -k^u \bar{g} \sum_{\ell=0}^{n} \sum_{p=-\infty}^{\infty} \hat{u}_{\ell,p} \frac{(k^u f)^{n-\ell}}{(n-\ell)!} \frac{H_p^{(n+1-\ell)}(k^u \bar{g})}{H_p(k^u \bar{g})} e^{ip\theta} - \frac{f}{\bar{g}} G_{n-1}^{(u)}(f)[U]$$

$$- 2k^u f \sum_{\ell=0}^{n-1} \sum_{p=-\infty}^{\infty} \hat{u}_{\ell,p} \frac{(k^u f)^{n-1-\ell}}{(n-1-\ell)!} \frac{H_p^{(n-\ell)}(k^u \bar{g})}{H_p(k^u \bar{g})} e^{ip\theta}$$

$$- \frac{k^u}{\bar{g}} f^2 \sum_{\ell=0}^{n-2} \sum_{p=-\infty}^{\infty} \hat{u}_{\ell,p} \frac{(k^u f)^{n-2-\ell}}{(n-2-\ell)!} \frac{H_p^{(n-1-\ell)}(k^u \bar{g})}{H_p(k^u \bar{g})} e^{ip\theta}$$

$$+ \frac{1}{\bar{g}} (f') \sum_{\ell=0}^{n-1} \sum_{p=-\infty}^{\infty} \hat{u}_{\ell,p} \frac{(k^u f)^{n-1-\ell}}{(n-1-\ell)!} \frac{H_p^{(n-1-\ell)}(k^u \bar{g})}{H_p(k^u \bar{g})} (ip) e^{ip\theta},$$

where the superscript in parentheses denotes derivative. Similar considerations hold for the DNO $G^{(w)}$

$$G_n^{(w)}(f)[W] = k^w \bar{g} \sum_{\ell=0}^{n} \sum_{p=-\infty}^{\infty} \hat{w}_{\ell,p} \frac{(k^w f)^{n-\ell}}{(n-\ell)!} \frac{J_p^{(n+1-\ell)}(k^w \bar{g})}{J_p(k^w \bar{g})} e^{ip\theta} - \frac{f}{\bar{g}} G_{n-1}^{(w)}(f)[W]$$

$$+ 2k^w f \sum_{\ell=0}^{n-1} \sum_{p=-\infty}^{\infty} \hat{w}_{\ell,p} \frac{(k^w f)^{n-1-\ell}}{(n-1-\ell)!} \frac{J_p^{(n-\ell)}(k^w \bar{g})}{J_p(k^w \bar{g})} e^{ip\theta}$$

$$+ \frac{k^w}{\bar{g}} f^2 \sum_{\ell=0}^{n-2} \sum_{p=-\infty}^{\infty} \hat{w}_{\ell,p} \frac{(k^w f)^{n-2-\ell}}{(n-2-\ell)!} \frac{J_p^{(n-1-\ell)}(k^u \bar{g})}{J_p(k^w \bar{g})} e^{ip\theta}$$

$$- \frac{1}{\bar{g}} (f') \sum_{\ell=0}^{n-1} \sum_{p=-\infty}^{\infty} \hat{w}_{\ell,p} \frac{(k^w f)^{n-1-\ell}}{(n-1-\ell)!} \frac{J_p^{(n-1-\ell)}(k^w \bar{g})}{J_p(k^w \bar{g})} (ip) e^{ip\theta},$$

c.f. [40].

3.4 The Method of Transformed Field Expansions

The method of Transformed Field Expansions proceeds in much the same way as the FE approach described above, save that a domain-flattening change of variables is effected prior to perturbation expansion [40,42]. For definiteness we consider the TFE method applied to the interior problem, (3.4), which we restate here for convenience,

$$
\begin{aligned}
\Delta w + \left(k^w\right)^2 w &= 0, & R_i &< r < \bar{g} + g(\theta), \\
w &= W, & r &= \bar{g} + g(\theta), \\
\partial_r w - T^{(w)}[w] &= 0, & r &= R_i.
\end{aligned}
$$

The change of variables we have in mind is

$$
r' = \frac{(\bar{g} - R_i)r + R_i g(\theta)}{\bar{g} + g(\theta) - R_i}, \quad \theta' = \theta,
$$

which maps the perturbed domain $\{R_i < r < \bar{g} + g(\theta)\}$ to the separable one $\{R_i < r' < \bar{g}\}$. This transformation changes the field w into

$$
v(r', \theta') := w\left(\frac{(\bar{g} + g(\theta') - R_i)r' - R_i g(\theta')}{\bar{g} - R_i}, \theta'\right),
$$

and modifies (3.4) to

$$
\begin{aligned}
\Delta v + \left(k^w\right)^2 v &= F(r, \theta; g), & R_i &< r < \bar{g}, & \text{(3.12a)} \\
v &= W, & r &= \bar{g}, & \text{(3.12b)} \\
\partial_r v - T^{(w)}[v] &= K(\theta; g), & r &= R_i, & \text{(3.12c)}
\end{aligned}
$$

where we have dropped the primed notation for clarity. It is not difficult to see that

$$
\begin{aligned}
-(\bar{g} - R_i)^2 F ={}& g(\bar{g} - R_i)(r - R_i)\partial_r[r\partial_r v] + g(\bar{g} - R_i)r\partial_r[(r - R_i)\partial_r v] \\
&+ g^2(r - R_i)\partial_r[(r - R_i)\partial_r v] + g(\bar{g} - R_i)\partial_\theta^2 v + (\bar{g} - R_i)\partial_\theta[g\partial_\theta v] + g\partial_\theta[g\partial_\theta v] \\
&- (g')(\bar{g} - R_i)(r - R_i)\partial_r\partial_\theta v - g(g')(r - R_i)\partial_r[\partial_\theta v] - g(g')\partial_\theta v \\
&- (\bar{g} - R_i)(r - R_i)\partial_\theta[(g')\partial_r v] - g(r - R_i)\partial_\theta[(g')\partial_r v] - (g')(\bar{g} - R_i)\partial_\theta v \\
&+ (g')^2(r - R_i)\partial_r[(r - R_i)\partial_r v] + (g')^2(r - R_i)\partial_r v + \sum_{j=1}^{4} C_j(g)(k^w)^2 v,
\end{aligned}
$$

with

$$
\begin{aligned}
C_1(g) &= g[2(\bar{g} - R_i)r^2 + 2(\bar{g} - R_i)(r - R_i)r], \\
C_2(g) &= g^2[r^2 + 4(r - R_i)r + (r - R_i)^2], \\
C_3(g) &= g^3\left[\frac{2}{(\bar{g} - R_i)}(r - R_i)r + \frac{2}{(\bar{g} - R_i)}(r - R_i)^2\right], \\
C_4(g) &= g^4\frac{1}{(\bar{g} - R_i)^2}(r - R_i)^2,
\end{aligned}
$$

and

$$
K = \frac{g}{\bar{g} - R_i}T^{(w)}[v].
$$

In addition we can recover that (3.5) changes to

$$G^{(w)}[W] = \frac{\bar{g} - R_i}{\bar{g} - R_i + g} \left[(\bar{g} + g) + \frac{(g')^2}{\bar{g} + g} \right] \partial_r v - \frac{g'}{\bar{g} + g} \partial_\theta v.$$

Upon setting $g = \varepsilon f$ and expanding

$$v(r, \theta, \varepsilon) = \sum_{n=0}^{\infty} v_n(r, \theta) \varepsilon^n,$$

we can show that

$$\Delta v_n + \left(k^w \right)^2 v_n = F_n, \qquad\qquad R_i < r < \bar{g}, \qquad (3.13a)$$
$$v_n = \delta_{n,0} W, \qquad\qquad r = \bar{g}, \qquad (3.13b)$$
$$\partial_r v_n - T^{(w)}[v_n] = K_n, \qquad\qquad r = R_i, \qquad (3.13c)$$

where

$$
\begin{aligned}
-(\bar{g} - R_i)^2 F_n =\ & f(\bar{g} - R_i)(r - R_i)\partial_r[r\partial_r v_{n-1}] + f(\bar{g} - R_i)r\partial_r[(r - R_i)\partial_r v_{n-1}] \\
& + f^2(r - R_i)\partial_r[(r - R_i)\partial_r v_{n-2}] + f(\bar{g} - R_i)\partial_\theta^2 v_{n-1} + (\bar{g} - R_i)\partial_\theta[f\partial_\theta v_{n-1}] \\
& + f\partial_\theta[f\partial_\theta v_{n-2}] - (f')(\bar{g} - R_i)(r - R_i)\partial_r \partial_\theta v_{n-1} - f(f')(r - R_i)\partial_r[\partial_\theta v_{n-2}] \\
& - f(f')\partial_\theta v_{n-2} - (\bar{g} - R_i)(r - R_i)\partial_\theta[(f')\partial_r v_{n-1}] \\
& - f(r - R_i)\partial_\theta[(f')\partial_r v_{n-2}] - (f')(\bar{g} - R_i)\partial_\theta v_{n-2} \\
& + (f')^2(r - R_i)\partial_r[(r - R_i)\partial_r v_{n-2}] + (f')^2(r - R_i)\partial_r v_{n-2} \\
& + \sum_{j=1}^{4} C_j(f)(k^w)^2 v_{n-j},
\end{aligned}
$$

and

$$K_n = \frac{f}{\bar{g} - R_i} T^{(w)}[v_{n-1}].$$

In addition it is not difficult to see that

$$
\begin{aligned}
G_n^{(w)}[W] =\ & -f\left(\frac{1}{\bar{g}} + \frac{1}{\bar{g} - R_i}\right) G_{n-1}^{(w)}[W] - \frac{f^2}{\bar{g}(\bar{g} - R_i)} G_{n-2}^{(w)}[W] + \bar{g}\partial_r v_n \\
& + 2f\partial_r v_{n-1} + \frac{f^2 + (f')^2}{\bar{g}}\partial_r v_{n-2} - \frac{f'}{\bar{g}}\partial_\theta v_{n-1} - \frac{f(f')}{\bar{g}(\bar{g} - R_i)}\partial_\theta v_{n-2},
\end{aligned}
$$

so that, provided with the $\{v_n\}$, we can readily approximate the terms, $G_n^{(w)}$, in the Taylor series expansion of $G^{(w)}$.

4 Numerical Results

We now present results of simulations of our implementation of the algorithm outlined above. The scheme is essentially a High-Order Spectral (HOS) approach [10,12,16] with nonlinearities approximated by convolutions implemented by the Fast Fourier Transform algorithm.

4.1 Validation by the Method of Manufactured Solutions

Before proceeding to our results, we validate our code using the "Method of Manufactured Solutions" (MMS) [8,22,49,54–57]. To summarize the MMS, when solving a system of partial differential equations for an unknown, v, say

$$\mathcal{P}v = 0, \quad \text{in } \Omega, \tag{4.1a}$$

subject to boundary conditions, e.g.,

$$\mathcal{B}v = 0, \quad \text{at } \partial\Omega, \tag{4.1b}$$

it is typically just as easy to implement an algorithm to solve the "inhomogenous" versions of the above,

$$\mathcal{P}v = \mathcal{F}, \qquad\qquad \text{in } \Omega, \tag{4.2a}$$
$$\mathcal{B}v = \mathcal{J}, \qquad\qquad \text{at } \partial\Omega. \tag{4.2b}$$

In order to test an implementation, one begins with the "manufactured solution," $\tilde{v}$, and sets

$$\mathcal{F} := \mathcal{P}\tilde{v}, \quad \mathcal{J} := \mathcal{B}\tilde{v}.$$

Now, given this pair $\{\mathcal{F}, \mathcal{J}\}$ we have an *exact* solution to (4.2) against which we can compare our numerically simulated solution. While this provides no guarantee of a correct implementation, with a careful choice of $\tilde{v}$, e.g. one which displays the same qualitative behavior as solutions of (4.1), the approach can give great confidence in the accuracy of a scheme.

For the implementation in question we consider the 2π-periodic, outgoing solutions of the Helmholtz equation, (2.1a),

$$u^q(r, \theta) = A_u^q H_q(k^u r)e^{iq\theta}, \quad q \in \mathbf{Z}, \quad A_u^q \in \mathbf{C},$$

and the bounded counterpart for (2.1b)

$$w^q(r, \theta) = A_w^q J_q(k^w r)e^{iq\theta}, \quad q \in \mathbf{Z}, \quad A_w^q \in \mathbf{C}.$$

For a given choice of $f = f(\theta)$ we can compute, e.g., the exact exterior Neumann data

$$v^{\text{ex}}(\theta) := \left[-\partial_N u^q\right]_{r=\bar{g}+\varepsilon f(\theta)} = \tilde{U}(\theta).$$

4.2 Implementation and Error Measurement

The method we described in Sect. 3 is a Fourier collocation/Taylor method [43,46] enhanced by Padé summation [1]. In more detail we approximate $\{U, W\}$ by

$$U^{N_\theta, N}(r, \theta) := \sum_{n=0}^{N} \sum_{p=-N_\theta/2}^{N_\theta/2-1} \hat{U}_{n,p} e^{ip\theta} \varepsilon^n, \quad W^{N_\theta, N}(r, \theta) := \sum_{n=0}^{N} \sum_{p=-N_\theta/2}^{N_\theta/2-1} \hat{W}_{n,p} e^{ip\theta} \varepsilon^n.$$

We insert these into (3.10) for each $n = 0, \dots, N$ to determine $\{\hat{U}_{n,p}, \hat{W}_{n,p}\}$. As has been pointed out [40,43], the TFE approach to compute DNOs requires an additional discretization in the vertical direction which we achieve by a Chebyshev collocation approach.

An important consideration is how the Taylor series in ε are summed. To be specific, in simulating U we consider the truncation $U^{N_\theta, N}$, which amounts to the approximation

$$\hat{U}_p(\varepsilon) := \sum_{n=0}^{\infty} \hat{U}_{p,n} \varepsilon^n,$$

for $-N_\theta/2 \le p \le N_\theta/2 - 1$, by

$$\hat{U}_p^N(\varepsilon) := \sum_{n=0}^N \hat{U}_{p,n} \varepsilon^n.$$

The classical numerical analytic continuation technique of Padé approximation [1] has been successfully brought to bear upon HOPS methods in the past (see, e.g., [5,44]), and we advocate its use here. Padé approximation seeks to simulate the truncated Taylor series $\hat{U}_p^N(\varepsilon)$ by the rational function

$$[L/M](\varepsilon) := \frac{a^L(\varepsilon)}{b^M(\varepsilon)} = \frac{\sum_{\ell=0}^L a_\ell \varepsilon^\ell}{1 + \sum_{m=1}^M b_m \varepsilon^m} \tag{4.3}$$

where $L + M = N$ and

$$[L/M](\varepsilon) = \hat{U}_p^N(\varepsilon) + \mathcal{O}(\varepsilon^{L+M+1});$$

well-known formulas for the coefficients $\{a_\ell, b_m\}$ can be found in [1]. This approximant has remarkable properties of enhanced convergence, and we refer the interested reader to Sect. 2.2 of Baker and Graves-Morris [1] and the insightful calculations of Sect. 8.3 of Bender and Orszag [2] for a thorough discussion of the capabilities and limitations of Padé approximants. To close this section, we point out that we measure the relative errors

$$\text{Error}_{\text{rel}}^{\text{FE}} = \frac{\left| \nu^{\text{ex}} - \nu_{N_\theta, N}^{\text{FE}} \right|_{L^\infty}}{|\nu^{\text{ex}}|_{L^\infty}}, \quad \text{Error}_{\text{rel}}^{\text{TFE}} = \frac{\left| \nu^{\text{ex}} - \nu_{N_\theta, N_r, N}^{\text{TFE}} \right|_{L^\infty}}{|\nu^{\text{ex}}|_{L^\infty}}. \tag{4.4}$$

4.3 Convergence Study

For our convergence study we select the 2π-periodic and analytic function

$$f(\theta) = e^{\cos(\theta)}, \tag{4.5}$$

see Fig. 2, and with this we compute the exact surface current, ν^{ex}. We make the physical parameter choices

$$q = 2, \quad A_u^q = 2, \quad A_w^q = 1, \quad \bar{g} = 0.025, \quad \varepsilon = 0.002, \tag{4.6}$$

Fig. 2 Plot of the cross-section of a metallic nanorod (occupying S^w) shaped by $r = \bar{g} + \varepsilon \exp(\cos(\theta))$ ($\varepsilon = \bar{g}/5$) housed in a dielectric (occupying S^u) under plane-wave illumination with wavenumber $(\alpha, -\gamma^u)$. The dash-dot blue line depicts the unperturbed geometry, the circle $r = \bar{g}$ (Color figure online)
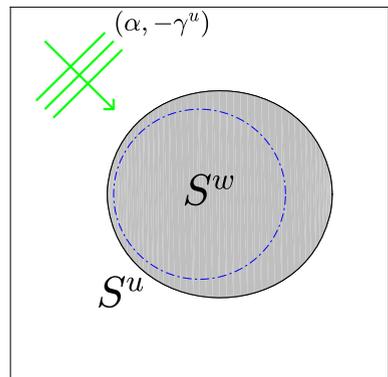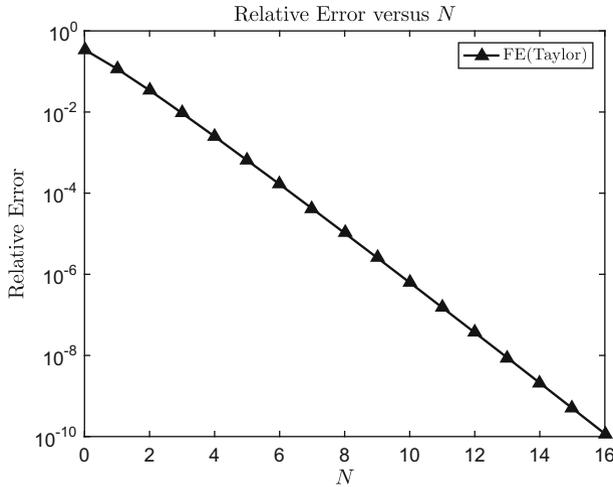
Fig. 3 Relative error (4.4) versus perturbation order for configuration (4.6); FE with Taylor summation
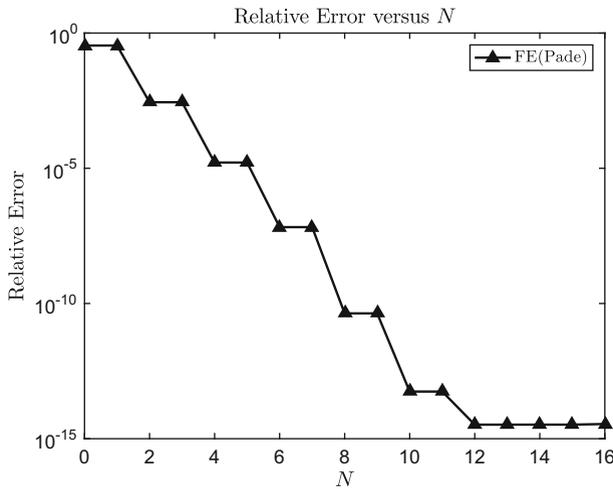
Fig. 4 Relative error (4.4) versus perturbation order for configuration (4.6); FE with Padé summation

and numerical parameter choices

$$N_\theta = 64, \quad N = 16, \tag{4.7}$$

and compute approximations to ν^{ex} by the FE algorithm delivering ν^{FE}.

In Figs. 3 and 4 we display results of our convergence study using Taylor and Padé summation, respectively. In these we see not only the reliability and robustness of our new approach, but also the extremely rapid, spectral, accuracy of our simulations.

We then reprise these calculations with a much larger choices of perturbation parameter, $\varepsilon = 0.01, 0.02, 0.05$. For this we used both the FE and TFE algorithms with the same choice of $f(\theta)$, (4.5), physical parameters, (4.6), and numerical parameters, (4.7), supplemented
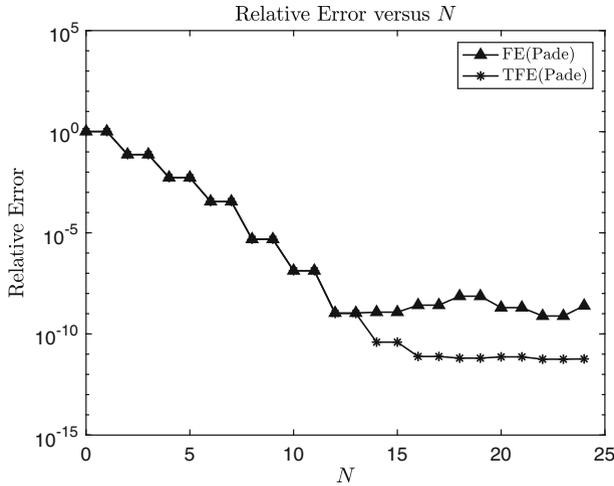
Fig. 5 Relative error (4.4) versus perturbation order for configuration (4.6); FE and TFE with Padé summation, $\varepsilon = 0.01$
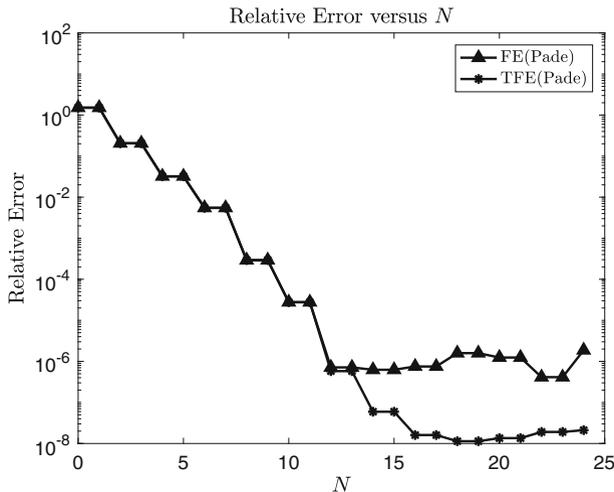
Fig. 6 Relative error (4.4) versus perturbation order for configuration (4.6); FE and TFE with Padé summation, $\varepsilon = 0.02$

with

$$\bar{g} = 0.025, \quad R_i = \bar{g}/10, \quad R^o = 10\bar{g}, \quad N_r = 64, \quad N = 24.$$

We compute approximations $\{v^{FE}, v^{TFE}\}$ and report results of our convergence study using Padé summation in Figs. 5, 6, and 7, for $\varepsilon = 0.01, 0.02$, and 0.05, respectively. Again, the fidelity and utility of both approaches is clearly visible in each, but we note the added accuracy and stability which TFE can provide.
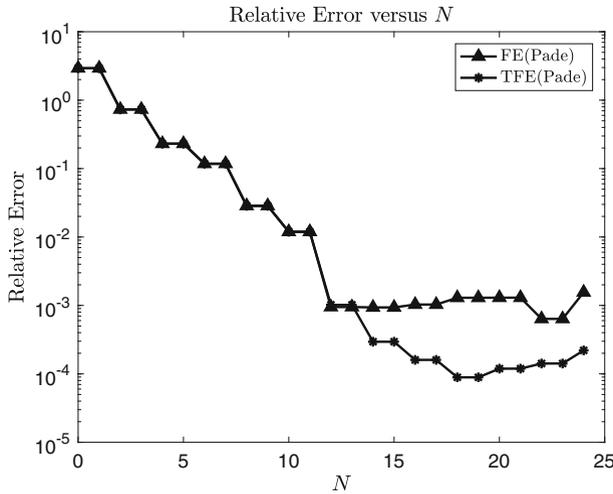
Fig. 7 Relative error (4.4) versus perturbation order for configuration (4.6); FE and TFE with Padé summation, $\varepsilon = 0.05$

4.4 Simulation of Nanorods

We now return to the problem of scattering of plane-wave incident radiation $u^{\text{inc}} = \exp(i\alpha x - i\gamma^u z)$ by a nanorod which demands the Dirichlet and Neumann conditions, (2.1c) and (2.1d) respectively. More specifically, we consider metallic nanorods housed in a dielectric with outer interface shaped by

$$r = \bar{g} + g(\theta) = \bar{g} + \varepsilon f(\theta).$$

We illuminate this structure over a range of incident wavelengths $\lambda_{min} \leq \lambda \leq \lambda_{max}$ and perturbation sizes $\varepsilon_{min} \leq \varepsilon \leq \varepsilon_{max}$, and compute the magnitudes of the reflected and transmitted surface currents, $\tilde{U}$ and $\tilde{W}$. These we term the "Reflection Map" (RM) and "Transmission Map" (TM) in analogy with similar quantities of interest in the study of metallic gratings [13,26,36,51]. Our study of the Fröhlich condition, (3.9), indicates that there should be a sizable enhancement in each at an LSPR. In the case of a nanorod with a perfectly circular cross-section we computed the value as the λ_F satisfying (3.9), and in subsequent plots this is depicted by a dashed red line.

4.4.1 An Analytic Deformation

Using the FE approach to compute the DNOs, we begin our study with the 2π-periodic and analytic profile from Sect. 4.3

$$f(\theta) = e^{\cos(\theta)}, \tag{4.8}$$

see Fig. 2. With this we consider the following physical configuration

$$\bar{g} = 0.025, \quad n^u = 1, \quad n^w = n^{\text{Ag}},$$
$$\lambda_{min} = 0.300, \quad \lambda_{max} = 0.800, \quad \varepsilon_{min} = 0, \quad \varepsilon_{max} = \bar{g}/10, \tag{4.9}$$

so that a silver (Ag) nanorod sits in vacuum, with numerical parameters

$$N_\lambda = 201, \quad N_\varepsilon = 201, \quad N_\theta = 64, \quad N = 16. \tag{4.10}$$
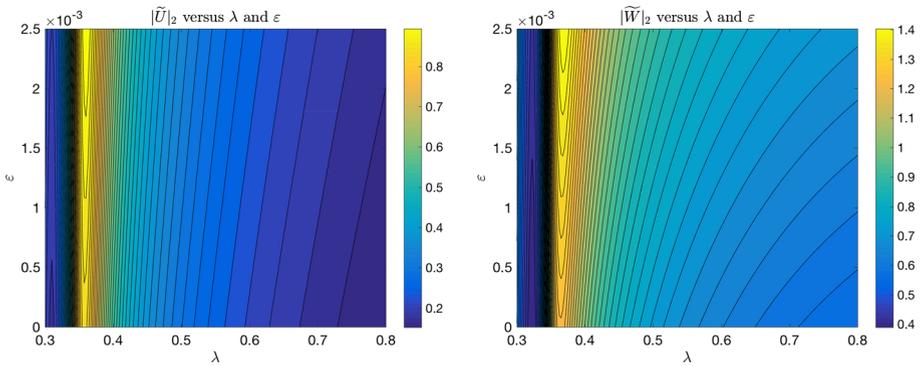
Fig. 8 Reflection Map and Transmission Map for a silver nanorod shaped by the analytic profile, (4.8), in vacuum. Here $\varepsilon_{max} = \bar{g}/10$, $\bar{g} = 0.025$, $\lambda_{min} = 0.300$, and $\lambda_{max} = 0.800$
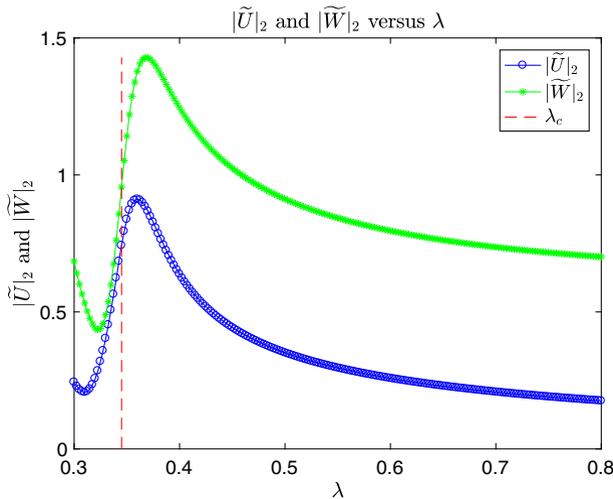
Fig. 9 Final Slice of Reflection and Transmission Maps at $\varepsilon = \varepsilon_{max}$ for a silver nanorod shaped by the analytic profile, (4.8), in vacuum

Plots of the RM and TM are displayed in Fig. 8. In Fig. 9 we show the final slice ($\varepsilon = \varepsilon_{max}$) of each of these, together with the Fröhlich value of the LSPR, (3.9), as a dashed red line. Here we see how even a relatively moderate value of the deformation parameter (one tenth of the rod radius) can produce a sizable shift in the LSPR location.

We revisit these calculations with three fundamental changes to the configuration (4.9): (i) boundary perturbation of twice the size ($\varepsilon_{max} = \bar{g}/5$), (ii) water as the host dielectric ($n^u = n^{\text{water}}$), and (iii) doubled boundary deformation in water. To summarize the effects of these changes, we present in Fig. 10 a collection of the final slices of RM and TM at $\varepsilon = \varepsilon_{max}$. Here we see that not only does an increase in the deformation size move the LSPR further away from the Fröhlich value, but also placing the nanorod in water spreads out the LSPR response in a significant way. Importantly, these results are easily generated with our method and show how useful our approach can be in the evaluation and design of nanorod structures.
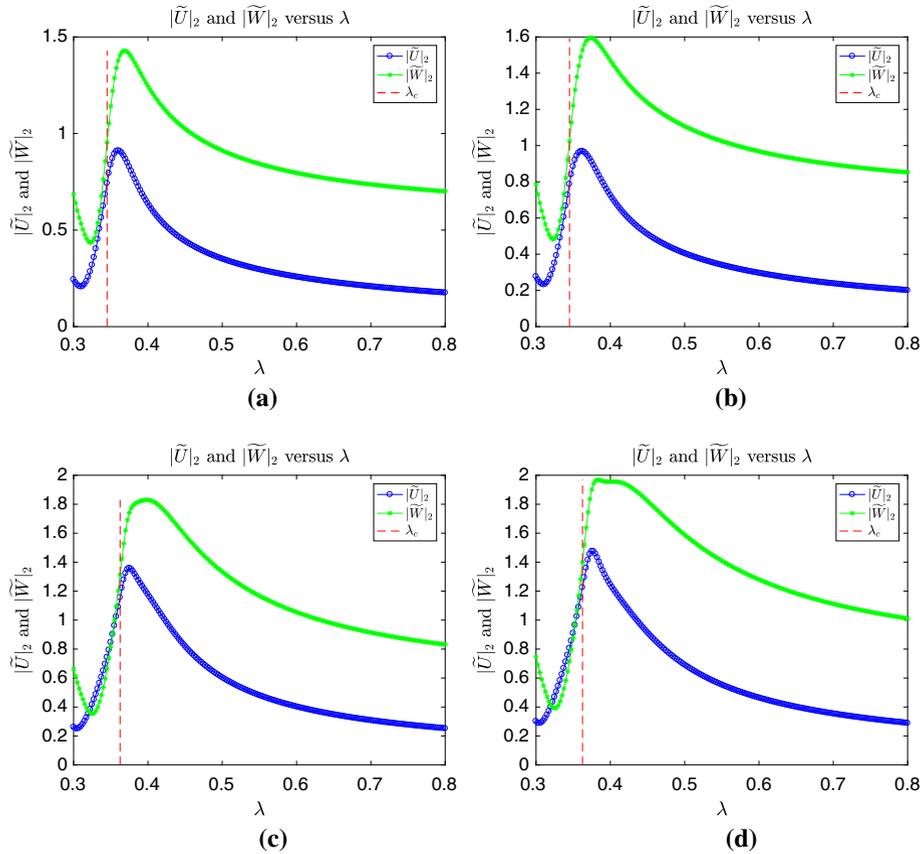
Fig. 10 Final slices of Reflection Maps and Transmission Maps for a silver nanorod shaped by the analytic profile, (4.8). **a** $\varepsilon = \bar{g}/10$ in vacuum; **b** $\varepsilon = \bar{g}/5$ in vacuum; **c** $\varepsilon = \bar{g}/10$ in water; **d** $\varepsilon = \bar{g}/5$ in water

4.4.2 A Low-Frequency Cosine Deformation

Continuing with the FE recursions, we consider the 2π-periodic, low-frequency sinusoidal profile

$$f(\theta) = \cos(2\theta), \tag{4.11}$$

see Fig. 11. Once again we consider the physical configuration (4.9) with numerical parameters (4.10).

Plots of the RM and TM are displayed in Fig. 12. In Fig. 13 we show the final slice ($\varepsilon = \varepsilon_{max}$) of each of these, together with the Fröhlich value of the LSPR, (3.9), as a dashed red line. As before, even a small perturbation in the deformation can move the LSPR shift in a noticeable way.

Once again, we study these calculations with three fundamental changes to the configuration (4.9): (i) boundary perturbation of twice the size ($\varepsilon_{max} = \bar{g}/5$), (ii) water as the host dielectric ($n^u = n^{water}$), and (iii) doubled boundary deformation in water. To summarize the effects of these changes, we present in Fig. 14 a collection of the final slices of RM and TM at $\varepsilon = \varepsilon_{max}$. Once again, we see that not only does an increase in the deformation size move

Fig. 11 Plot of the cross-section of a metallic nanorod (occupying S^w) shaped by $r = \bar{g} + \varepsilon \cos(2\theta)$ ($\varepsilon = \bar{g}/5$) housed in a dielectric (occupying S^u) under plane-wave illumination with wavenumber $(\alpha, -\gamma^u)$. The dash-dot blue line depicts the unperturbed geometry, the circle $r = \bar{g}$ (Color figure online)
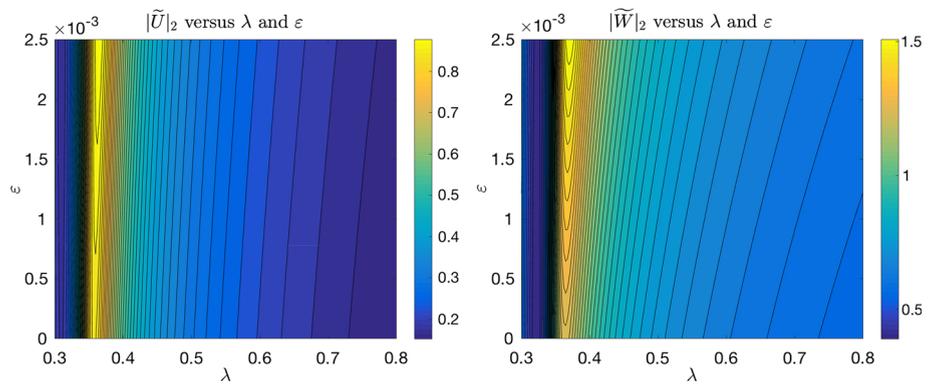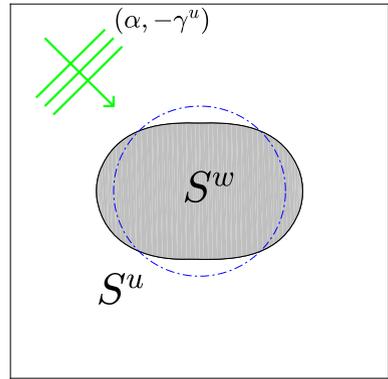
Fig. 12 Reflection Map and Transmission Map for a silver nanorod shaped by the sinusoidal profile, (4.11), in vacuum. Here $\varepsilon_{max} = \bar{g}/10$, $\bar{g} = 0.025$, $\lambda_{min} = 0.300$, and $\lambda_{max} = 0.800$
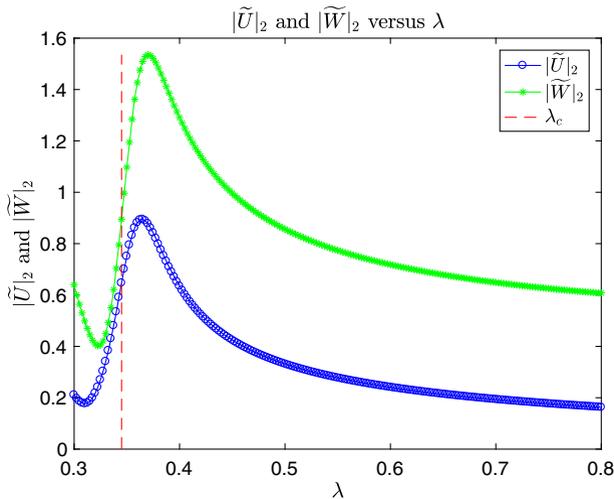
Fig. 13 Final Slice of Reflection and Transmission Maps at $\varepsilon = \varepsilon_{max}$ for a silver nanorod shaped by the sinusoidal profile, (4.11), in vacuum
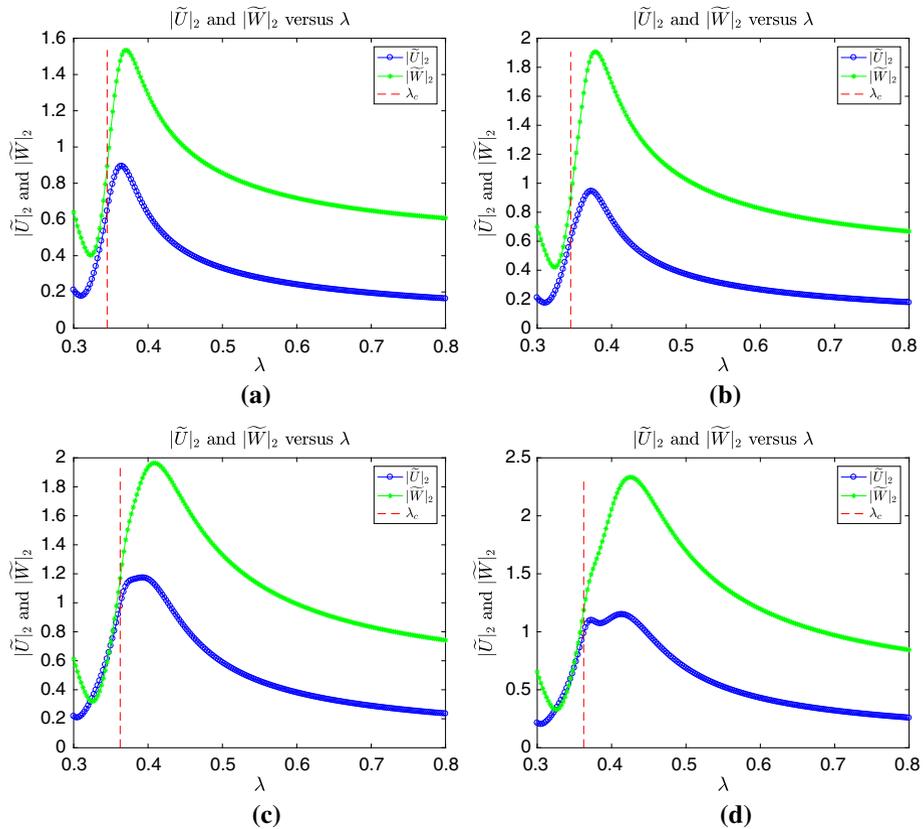
Fig. 14 Final slices of Reflection Maps and Transmission Maps for a silver nanorod shaped by the sinusoidal profile, (4.11). **a** $\varepsilon = \bar{g}/10$ in vacuum; **b** $\varepsilon = \bar{g}/5$ in vacuum; **c** $\varepsilon = \bar{g}/10$ in water; **d** $\varepsilon = \bar{g}/5$ in water

the LSPR further away from the Fröhlich value, but also placing the nanorod in water spreads out the LSPR response (though not as severely as for the analytic profile), while giving rise to a "double-peak" in water.

4.4.3 A Higher Frequency Cosine Deformation

Once again with the FE approach, we conclude with the 2π-periodic sinusoidal profile of slightly higher frequency

$$f(\theta) = \cos(4\theta), \tag{4.12}$$

see Fig. 15. Once again we consider the physical configuration (4.9) with numerical parameters (4.10).

Plots of the RM and TM are displayed in Fig. 16. In Fig. 17 we show the final slice ($\varepsilon = \varepsilon_{max}$) of each of these, together with the Fröhlich value of the LSPR, (3.9), as a dashed red line. Unsurprisingly, we notice how even a moderate value of the deformation parameter delivers a sizable shift in the LSPR location.

Once again, we study these calculations with three fundamental changes to the configuration (4.9): (i) boundary perturbation of twice the size ($\varepsilon_{max} = \bar{g}/5$), (ii) water as the host

Fig. 15 Plot of the cross-section of a metallic nanorod (occupying S^w) shaped by $r = \bar{g} + \varepsilon \cos(4\theta)$ ($\varepsilon = \bar{g}/5$) housed in a dielectric (occupying S^u) under plane-wave illumination with wavenumber $(\alpha, -\gamma^u)$. The dash-dot blue line depicts the unperturbed geometry, the circle $r = \bar{g}$ (Color figure online)
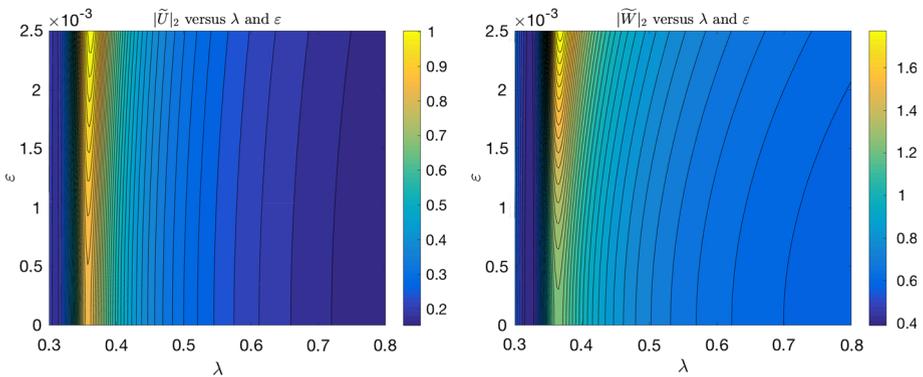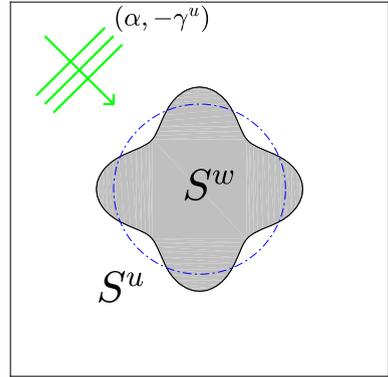
Fig. 16 Reflection Map and Transmission Map for a silver nanorod shaped by the sinusoidal profile, (4.12), in vacuum. Here $\varepsilon_{max} = \bar{g}/10$, $\bar{g} = 0.025$, $\lambda_{min} = 0.300$, and $\lambda_{max} = 0.800$
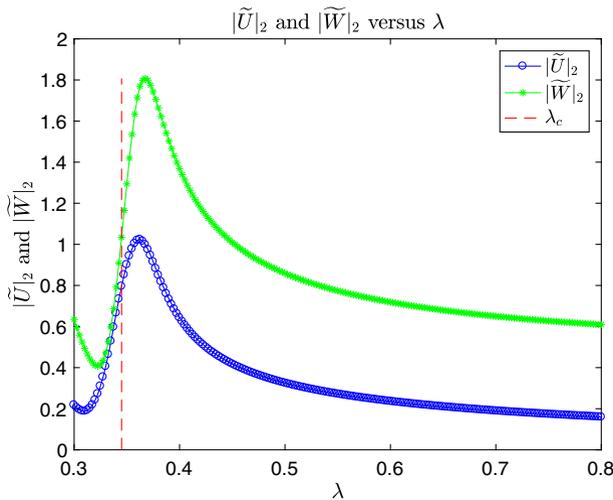
Fig. 17 Final Slice of Reflection and Transmission Maps at $\varepsilon = \varepsilon_{max}$ for a silver nanorod shaped by the sinusoidal profile, (4.12), in vacuum
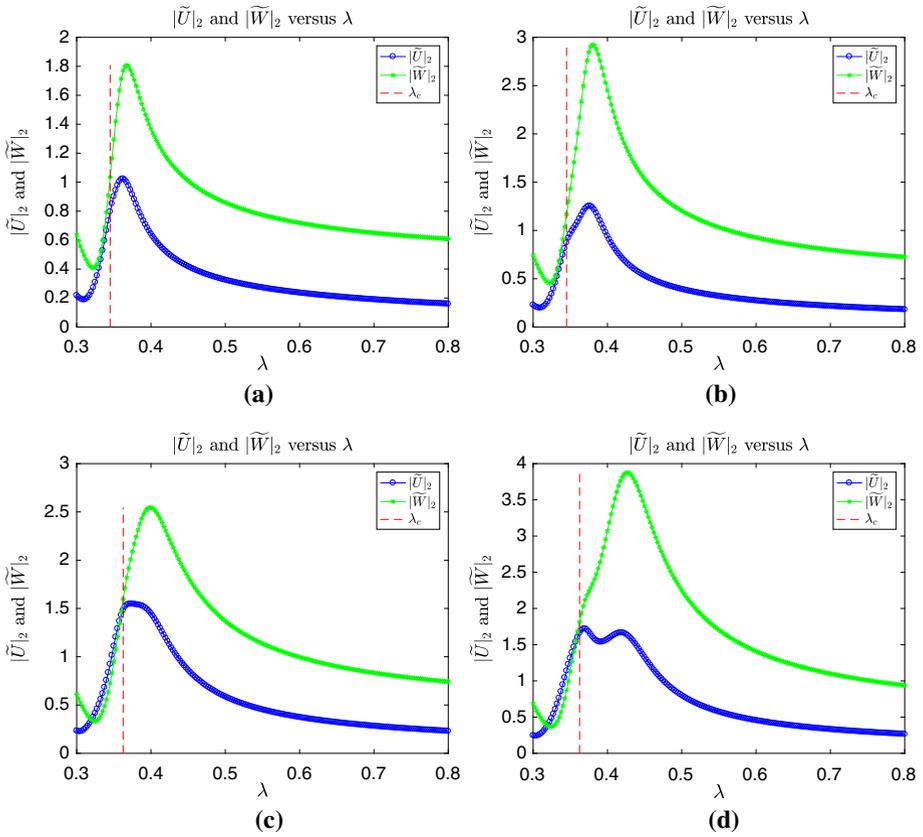
Fig. 18 Final slices of Reflection Maps and Transmission Maps for a silver nanorod shaped by the sinusoidal profile, (4.12). **a** $\varepsilon = \bar{g}/10$ in vacuum; **b** $\varepsilon = \bar{g}/5$ in vacuum; **c** $\varepsilon = \bar{g}/10$ in water; **d** $\varepsilon = \bar{g}/5$ in water

dielectric ($n^u = n^{\text{water}}$), and (iii) doubled boundary deformation in water. To summarize the effects of these changes, we present in Fig. 18 a collection of the final slices of RM and TM at $\varepsilon = \varepsilon_{max}$. In this third case we see that an increase in the deformation size moves the LSPR further away from the Fröhlich value, and placing the nanorod in water not only spreads out the LSPR response, but also creates a "bifurcation" in the response.

Before closing we illustrate the enhanced accuracy and stability which can be realized with the TFE recursions. The FE approach delivers high-fidelity results over a wide range of parameter choices including all of the simulations presented here, however, there is a limit to the accuracy which can be achieved. This is due to subtle cancellations in the FE recursions which render the computations ill-conditioned for extreme configurations [43,45]. In contrast, while having a slightly elevated operation count, the TFE formulas stably deliver accurate solutions in configurations where the FE counterparts display disappointing performance. To highlight this latter issue we examine the highly oscillatory sinusoidal profile

$$f(\theta) = \cos(8\theta), \tag{4.13}$$

for which we could not uniformly resolve the solution with our FE approach at $\varepsilon = \bar{g}/10$. We focus upon the particular value $\lambda = 0.3875$ for the water/silver configuration we investigated

Table 1 L^2 norm of $\tilde{U}^N$, Q_N, versus perturbation order, N, for the water/silver configuration with $f(\theta) = \cos(8\theta)$ with FE and TFE algorithms

N	Q_N^{FE}	$\left| Q_N^{\text{FE}} - Q_{N-4}^{\text{FE}} \right|$	Q_N^{TFE}	$\left| Q_N^{\text{TFE}} - Q_{N-4}^{\text{TFE}} \right|$
0	1.210354021216885		1.210354021216792	
4	2.644285028038841	0.837088	2.633537216442172	0.847836
8	2.563745050094514	0.08054	2.386786362653798	0.246751
16	13.7218584661541	11.1581	2.225590119856692	0.161196
20	4.804761546058774	8.9171	2.227441479239038	0.00185136
24	4.10503488514615	0.699727	2.227341193552773	0.000100286

earlier. In Table 1 we report the L^2 norm of $\tilde{U}$,

$$Q_N := \left\| \tilde{U}^N \right\|_{L^2}, \tag{4.14}$$

as a function of perturbation order, N, to sixteen digits. We see that not only does the FE algorithm deliver rather poor results (no more than one digit of accuracy), but also that our TFE recursions give us a reasonable approximation (three to four digits of accuracy).

5 Conclusion

In this contribution we have developed a novel computational methodology to study the LSPRs which can be induced in silver nanorods with visible light, and how they change as the shapes of these rods are varied analytically away from perfectly cylindrical. Our HOPS approach, while closely related to the work of Bruno and Reitich [7], differs in a number of ways beginning with its two-dimensional character and formulation in terms of DNOs first described in [37] which permits the immediate simulation by any of classical (OE or FE) or stabilized (TFE) HOPS methods. In this contribution we provided not only a detailed prescription of the algorithm, but also validated the scheme. With numerical experiments we showed the remarkable efficiency, fidelity, and high-order accuracy one can achieve with an implementation of this algorithm.

References

1. Baker Jr., George A.: Padé Approximants, 2nd edn. Cambridge University Press, Cambridge (1996)
2. Bender, Carl M, Orszag, Steven A: Advanced Mathematical Methods for Scientists and Engineers. McGraw-Hill Book Co, New York (1978). International Series in Pure and Applied Mathematics
3. Boyd, John P.: Chebyshev and Fourier Spectral Methods, 2nd edn. Dover Publications Inc., Mineola (2001)
4. Bruno, O., Reitich, F.: Numerical solution of diffraction problems: a method of variation of boundaries. J. Opt. Soc. Am. A **10**(6), 1168–1175 (1993)
5. Bruno, O., Reitich, F.: Numerical solution of diffraction problems: a method of variation of boundaries. II. Finitely conducting gratings, Padé approximants, and singularities. J. Opt. Soc. Am. A **10**(11), 2307–2316 (1993)

6. Bruno, O., Reitich, F.: Numerical solution of diffraction problems: a method of variation of boundaries. III. Doubly periodic gratings. J. Opt. Soc. Am. A **10**(12), 2551–2562 (1993)
7. Bruno, Oscar P., Reitich, Fernando: Boundary-variation solutions for bounded-obstacle scattering problems in three dimensions. J. Acoust. Soc. Am. **104**(5), 2579–2583 (1998)
8. Burggraf, O.R.: Analytical and numerical studies of the structure of steady separated flows. J. Fluid Mech. **24**, 113–151 (1966)
9. Coifman, R., Goldberg, M., Hrycak, T., Israeli, M., Rokhlin, V.: An improved operator expansion algorithm for direct and inverse scattering computations. Waves Random Media **9**(3), 441–457 (1999)
10. Canuto, C., Hussaini, M.Y., Quarteroni, A., Zang, T.A.: Spectral Methods in Fluid Dynamics. Springer, New York (1988)
11. Colton, D., Kress, R.: Inverse Acoustic and Electromagnetic Scattering Theory, 2nd edn. Springer, Berlin (1998)
12. Deville, M.O., Fischer, P.F., Mund, E.H.: High-Order Methods for Incompressible Fluid Flow, volume 9 of Cambridge Monographs on Applied and Computational Mathematics. Cambridge University Press, Cambridge (2002)
13. Enoch, S., Bonod, N.: Plasmonics: From Basics to Advanced Topics. Springer Series in Optical Sciences. Springer, New York (2012)
14. El-Sayed, I., Huang, X., El-Sayed, M.: Selective laser photo-thermal therapy of epithelial carcinoma using anti-egfr antibody conjugated gold nanoparticles. Cancer Lett. **239**(1), 129–135 (2006)
15. Evans, Lawrence C.: Partial Differential Equations, 2nd edn. American Mathematical Society, Providence (2010)
16. Gottlieb, D., Orszag, S.A.: Numerical analysis of spectral methods: theory and applications. Society for Industrial and Applied Mathematics, Philadelphia, Pa. (1977). CBMS-NSF Regional Conference Series in Applied Mathematics, No. 26
17. Greengard, L., Rokhlin, V.: A fast algorithm for particle simulations. J. Comput. Phys. **73**(2), 325–348 (1987)
18. Hu, B., Nicholls, D.P.: Analyticity of Dirichlet–Neumann operators on Hölder and Lipschitz domains. SIAM J. Math. Anal. **37**(1), 302–320 (2005)
19. Hesthaven, J.S., Warburton, T.: Nodal discontinuous Galerkin methods, volume 54 of Texts in Applied Mathematics. In: Algorithms, analysis, and applications. Springer, New York (2008)
20. Ihlenburg, Frank: Finite Element Analysis of Acoustic Scattering. Springer, New York (1998)
21. Johnson, Claes: Numerical Solution of Partial Differential Equations by the Finite Element Method. Cambridge University Press, Cambridge (1987)
22. Knupp, P., Salari, K.: Verification of Computer Codes in Computational Science and Engineering. Chapman and Hall/CRC, Boca Raton (2003)
23. LeVeque, Randall J.: Finite difference methods for ordinary and partial differential equations. In: Steady-state and time-dependent problems. Society for Industrial and Applied Mathematics (SIAM), Philadelphia (2007)
24. Liu, M., Guyot-Sionnest, P., Lee, T.-W., Gray, S.: Optical properties of rodlike and bipyramidal gold nanoparticles from three-dimensional computations. Phys. Rev. B **76**, 235428 (2007)
25. Loo, C., Lowery, A., Halas, N., West, J., Drezek, R.: Immunotargeted nanoshells for integrated cancer imaging and therapy. Nano Lett. **5**(4), 709–711 (2005)
26. Maier, S.A.: Plasmonics: Fundamentals and Applications. Springer, New York (2007)
27. Martin, P.A.: Multiple scattering, volume 107 of Encyclopedia of Mathematics and its Applications. In: Interaction of time-harmonic waves with N obstacles. Cambridge University Press, Cambridge (2006)
28. Myroshnychenko, V., Carbo-Argibay, E., Pastoriza-Santos, I., Perez-Juste, J., Liz-Marzan, L., Garcia de Abajo, F.: Modeling the optical response of highly faceted metal nanoparticles with a fully 3d boundary element method. Adv. Mater. **20**, 4288–4293 (2008)
29. Milder, D. M.: An improved formalism for rough-surface scattering of acoustic and electromagnetic waves. In: Proceedings of SPIE—The International Society for Optical Engineering (San Diego, 1991), volume 1558, pp. 213–221. International Society for Optical Engineering, Bellingham (1991)
30. Milder, D. M.: An improved formalism for wave scattering from rough surfaces. J. Acoust. Soc. Am. **89**(2), 529–541 (1991)
31. Milder, D. M.: An improved formalism for electromagnetic scattering from a perfectly conducting rough surface. Radio Sci. **31**(6), 1369–1376 (1996)
32. Milder, D. M.: Role of the admittance operator in rough-surface scattering. J. Acoust. Soc. Am. **100**(2), 759–768 (1996)
33. Myroshnychenko, V., Rodriguez-Fernandez, J., Pastoriza-Santos, I., Funston, A., Novo, C., Mulvaney, P., Liz-Marzan, L., Garcia de Abajo, J.: Modelling the optical response of gold nanoparticles. Chem. Soc. Rev. **37**, 1792–1805 (2008)

34. Milder, D. M., Sharp, H. Thomas: Efficient computation of rough surface scattering. In: Mathematical and Numerical Aspects of Wave Propagation Phenomena (Strasbourg, 1991), pp. 314–322. SIAM, Philadelphia (1991)
35. Milder, D. M., Sharp, H.Thomas: An improved formalism for rough surface scattering. ii: Numerical trials in three dimensions. J. Acoust. Soc. Am. **91**(5), 2620–2626 (1992)
36. Novotny, L., Hecht, B.: Principles of Nano-Optics, 2nd edn. Cambridge University Press, Cambridge (2012)
37. Nicholls, D.P.: Three-dimensional acoustic scattering by layered media: a novel surface formulation with operator expansions implementation. Proc. R. Soc. Lond. A **468**, 731–758 (2012)
38. Nicholls, D.P.: A method of field expansions for vector electromagnetic scattering by layered periodic crossed gratings. J. Opt. Soc. Am. A **32**(5), 701–709 (2015)
39. Nicholls, D.P.: On analyticity of linear waves scattered by a layered medium. J. Differ. Equ. **263**(8), 5042–5089 (2017)
40. Nicholls, D.P., Nigam, N.: Exact non-reflecting boundary conditions on general domains. J. Comput. Phys. **194**(1), 278–303 (2004)
41. Nicholls, D.P., Oh, S.-H., Johnson, T.W., Reitich, F.: Launching surface plasmon waves via vanishingly small periodic gratings. J. Opt. Soc. Am. A **33**(3), 276–285 (2016)
42. Nicholls, D.P., Reitich, F.: A new approach to analyticity of Dirichlet–Neumann operators. Proc. R. Soc. Edinb. Sect. A **131**(6), 1411–1433 (2001)
43. Nicholls, D.P., Reitich, F.: Stability of high-order perturbative methods for the computation of Dirichlet–Neumann operators. J. Comput. Phys. **170**(1), 276–298 (2001)
44. Nicholls, D.P., Reitich, F.: Analytic continuation of Dirichlet–Neumann operators. Numer. Math. **94**(1), 107–146 (2003)
45. Nicholls, D.P., Reitich, F.: Shape deformations in rough surface scattering: cancellations, conditioning, and convergence. J. Opt. Soc. Am. A **21**(4), 590–605 (2004)
46. Nicholls, D.P., Reitich, F.: Shape deformations in rough surface scattering: improved algorithms. J. Opt. Soc. Am. A **21**(4), 606–621 (2004)
47. Nicholls, D.P., Shen, J.: A stable, high-order method for two-dimensional bounded-obstacle scattering. SIAM J. Sci. Comput. **28**(4), 1398–1419 (2006)
48. Nicholls, D.P., Tammali, V.: A high-order perturbation of surfaces (hops) approach to Fokas integral equations: vector electromagnetic scattering by periodic crossed gratings. Appl. Numer. Methods **101**, 1–17 (2016)
49. Oberkampf, W.L., Trucano, T.G., Hirsch, C.: Verification, validation, and predictive capability in computational engineering and physics. Appl. Mech. Rev. **57**(5), 345–384 (2004)
50. Petit, R. (ed.): Electromagnetic Theory of Gratings. Springer, Berlin (1980)
51. Raether, H.: Surface Plasmons on Smooth and Rough Surfaces and on Gratings. Springer, Berlin (1988)
52. Rayleigh, Lord: On the dynamical theory of gratings. Proc. R. Soc. Lond. **A79**, 399–416 (1907)
53. Rice, S.O.: Reflection of electromagnetic waves from slightly rough surfaces. Commun. Pure Appl. Math. **4**, 351–378 (1951)
54. Roache, P.J.: Verification and Validation in Computational Science and Engineering. Hermosa Publishers, Albuquerque (1998)
55. Roache, P.J.: Verification of codes and calculations. AIAA J. **36**(5), 696–702 (1998)
56. Roache, P.J.: Code verification by the method of manufactured solutions. J. Fluids Eng. **124**(1), 4–10 (2002)
57. Roy, C.J.: Review of code and solution verification procedures for computational simulation. J. Comput. Phys. **205**(1), 131–156 (2005)
58. Reitich, F., Tamma, K.: State-of-the-art, trends, and directions in computational electromagnetics. CMES Comput. Model. Eng. Sci. **5**(4), 287–294 (2004)
59. Strikwerda, John C.: Finite Difference Schemes and Partial Differential Equations, 2nd edn. Society for Industrial and Applied Mathematics (SIAM), Philadelphia (2004)
60. Xu, H., Bjerneld, E., Käll, M., Börjesson, L.: Spectroscopy of single hemoglobin molecules by surface enhanced raman scattering. Phys. Rev. Lett. **83**, 4357–4360 (1999)